

**Scanning probe anodization patterning of Si substrates covered with a self-assembled monolayer dependent on hydrophilicity**

Jiwon HAN, Daiji KASAHARA, Takashi ICHII, Kuniaki MURASE, and  
Hiroyuki SUGIMURA\*

Department of Materials Science and Engineering, Kyoto University,  
Sakyo, Kyoto 606-8501, Japan.

\*E-mail address: [Hiroyuki.Sugimura@materials.mbox.media.kyoto-u.ac.jp](mailto:Hiroyuki.Sugimura@materials.mbox.media.kyoto-u.ac.jp)

**MATERIALS**

Silicon, undecene, diamond

**ABSTRACT**

Contact-mode atomic force microscopy (AFM)-based anodization patterning was performed on Si substrates covered with a self-assembled monolayer (SAM) to investigate effects of relative humidity (RH), surface wettability of the SAM, and probe-tip material on widths and heights of drawn lines. Three types of SAMs, that is, methyl-terminated, ester-terminated, and carboxyl-terminated SAMs, were prepared on hydrogen-terminated silicon (Si) substrates by a thermal activation method. These SAMs were covalently fixed on the Si substrates through Si-C bonds without an interfacial oxide layer between the SAM and Si. Rh-coated and boron-doped conductive diamond-

coated AFM probe-tips were used for patterning with a positive sample bias of 10 V. Consequently, the region scanned with the AFM probe became protruded due to degradation of the SAM and anodization of Si. When the Rh-coated tip was used, the width of the protruded line increased with increasing RH on each SAM sample. The line width on the most hydrophilic methyl-terminated SAM was narrowest, while that on the most hydrophilic carboxylic SAM was widest. However there was no distinct difference in the pattern width at the patterning under low RH of 10 %. In the case of patterning with the boron-doped conductive diamond-coated tip on the ester-SAM, the width of the patterned line showed no clear increase with increasing RH. These pattern width changes were discussed in terms of the size of adsorbed water meniscus at the AFM-tip/sample junction as confirmed by force curve measurements; in the case of the diamond tip which is rather more hydrophobic than the Rh-coated tip, the size of water meniscus hardly affected RH.

## **I. INTRODUCTION**

Technologies of microscopes have been frequently extended to micro - nanofabrication technologies. For example, electron beam lithography, which is the most successful nanofabrication technology, has been developed based on the technology of electron microscopy. Accordingly, the development of new microscope techniques pushes forward novel microfabrication/nanofabrication processes. Scanning probe microscopy (SPM) has been recognized as a

powerful nanoscopic tool for studies in surface science and engineering. Hence, as well as the other microscopes, SPM technologies have inevitably attracted much attention as nanofabrication tools since their birth.<sup>1-4</sup> There have been numerous reports on SPM-based nanofabrication using a variety of chemical and/or physical surface-modification mechanisms. Among these mechanisms, the local “oxidation” of a material surface induced at the SPM tip-sample junction, including scanning probe anodization,<sup>5</sup> is a promising technique. This technique is applicable to drawing nanopatterns on a wide variety of materials including metals, semiconductors, inorganic compounds and organic materials. In addition, the local “oxidation” can be conducted in an ambient condition by simply applying a bias voltage to a tip-sample junction. Scanning probe anodization is a particular nano-oxidation technique in which a substrate is biased positively in order to induce electrochemical oxidation reactions, that is, anodic reactions, on the substrate surface.<sup>6</sup>

Nanostructuring silicon (Si) surfaces by SPM is of central interest, since this material is one of the most important materials in micro ~ nano electronics. Accordingly, scanning probe anodization has been applied to nanopatterning of Si as well. Another interesting material for SPM-based nanopatterning is self-assembled monolayers (SAMs).<sup>7,8</sup> SAMs, that is, organic thin films of monomolecular thickness, are formed spontaneously on a substrate when specific molecules chemisorb on it. Organic nanostructures have been successfully fabricated through SPM patterning of SAMs. If we combine such a

SAM with a Si substrate and employ as a target sample for scanning probe anodization, we can expect to fabricate a wide variety of nanostructures on Si. Indeed, organosilane SAMs formed on Si substrates have been successfully nanostructured by scanning probe anodization and various pattern transfer processes have been demonstrated using a nanostructured SAM as a minute template. For example, SPM-patterned SAMs successfully served as resist masks for wet chemical etching in order to fabricate narrow grooves or minute holes on Si substrates.<sup>9,10</sup> Furthermore, metallic nanostructures consisting of Ni or Au were fabricated on Si surfaces by area-selective electroless plating in which nucleation sites were prepared by a lithographic technique based on SPM and organosilane SAMs.<sup>11-13</sup> Li et al. employed similar nanostructured SAMs as templates in order to assemble Au nanoparticles on specific areas on a SAM-covered Si substrate.<sup>14</sup> Besides metals, organic nanostructures consisting of more than two components have been fabricated as well. For example, a nanostructured sample composed of alkylsilane SAM and Si oxide was first prepared by scanning probe anodization of the SAM and then the oxide part of the sample surface was area-selectively modified with another organosilane SAM.<sup>15,16</sup> This second SAM was used in order to modify the local surface potential at nanoscale<sup>16</sup> or served as a crosslinker layer on which polymer nanoparticles or biomolecules were area-selectively immobilized.<sup>15</sup> Meanwhile, Sagiv and co-workers developed another SPM-based method to fabricate organic nanostructures.<sup>17,18</sup> An organic molecular bilayer was self-assembled

into a localized area on an organosilane SAM surface of which the top surface functional groups had been converted to be chemically active by SPM tip-induced local anodization.

Recently, alkyl SAMs directly attached to Si substrates typically through Si-C bonds have attracted attention as alternatives to organosilane SAMs,<sup>19</sup> because of their atomically flat surfaces,<sup>20</sup> thermal and chemical stability<sup>21,22</sup> and a similar patternability in scanning probe anodization.<sup>23-25</sup> Furthermore, advantages are provided from the characteristic of the direct-attach SAM/Si sample that there is no oxide layer between such a SAM and its Si substrate. The direct-attach SAM/Si sample can be anodized with a lower threshold bias than that for an organosilane SAM/Si sample which has an interfacial oxide layer at least 2 nm in thickness.<sup>24,25</sup> Charge traps which degrade the performance of Si electronic devices have been found to be not present at the SAM-Si interface, in contrast to the organosilane SAM/Si samples.<sup>26</sup>

Although scanning probe anodization has been successfully applied to nanopatterning of the direct-attach SAM/Si samples so far, there have been few studies from the view point of size control of the adsorbed water meniscus formed at the SPM-tip/sample junction in spite of its particular influence on the patterning resolution. In this study, therefore, we focused on the effects of relative humidity (RH), surface hydrophilicity of SAMs and probe-tip materials on scanning probe anodization of SAM-Si samples.

## II. EXPERIMENTAL

Three types of SAM-covered Si samples were prepared for this work. Prior to the SAM formation, Si substrates cut from an n-type Si (111) wafer with a resistivity of 1 - 10  $\Omega$  cm were cleaned by sonication in ethanol and ultrapure water in that order for 20 min, respectively. Then, carbonaceous contamination on the Si substrates was removed by a photochemical method using a light source radiating vacuum ultra violet at 172 nm in wavelength (Ushio UER20-172V; intensity at the lamp window, 10mW cm<sup>-2</sup>). The details of this photochemical cleaning method are described elsewhere.<sup>27</sup> Next, in order to remove surface oxide, cleaned Si substrates were treated in 5 % HF aqueous solution for 5 min at room temperature (RT) followed by 40 % NH<sub>4</sub>F aqueous solution for 30 sec at 80°C so that the Si substrate surfaces became terminated with hydrogen. Finally, onto each of these Si(111)-H substrates, a SAM was formed by a thermal activation method.<sup>28</sup> One of the Si-H samples was placed in a three-neck separable glass flask filled with 1M solution of 1-undecene in mesitylene kept at 150°C for 2 hours. The inside of the flask was purged with N<sub>2</sub> bubbling. Consequently, as illustrated in Fig. 1(c), an undecyl SAM, terminated with methyl groups, was formed on the substrate. Similarly, an ester-terminated SAM was formed in 1M solution of 10-undecenoic acid methyl ester in mesitylene on each of the other Si-H substrates as illustrated in Fig. 1(d). After the SAM formation processes, all the samples were rinsed by sonication in mesitylene, ethanol, and ultrapure water for 5 min each, in that order, and then

dried in a stream of N<sub>2</sub> gas. A sample coated with a carboxyl-terminated SAM was obtained by hydrolysis of the surface ester groups on the ester-terminated SAM as illustrated in Fig. 1(e). This process was conducted by treating the sample with a 0.25 M solution of potassium *tert*-butoxide in dimethyl sulfoxide for 10 min at RT, and with a 1 M HCl for 10 min at RT. After the treatment, the sample was sonicated in ultrapure water for 5 min and then dried in a stream of N<sub>2</sub> gas.<sup>29,30</sup> Water contact angles of the methyl-, ester-, and carboxyl-terminated SAMs were approximately 96°, 73°, and 53°, respectively. The thicknesses of the SAMs were all approximately 1.7 nm as measured by ellipsometry.

Patterning experiments were performed using a commercial AFM (SII NanoTechnology Inc., SPA-300HV + SPI-3800N) in contact mode under controlled atmospheric humidity by flowing air saturated with water vapor and dry air streams into a chamber where the AFM unit was located. The flow rate of each gas stream was adjusted by a regulator. The RH in the AFM chamber was monitored with 3% error in the range of 0 to 90% RH at room temperature by a precision hygrometer (MR6662, Chino, Japan). In this experiment, 10, 40, and 70% RH were subsequently adjusted at one-hour intervals for patterning. A sample bias voltage relative to the grounded probe tip was applied to the substrate Si of a SAM-covered sample. The probe was scanned at a scan rate of 0.5 μm/s with a bias of 10 V under a controlled RH of 10%, 40%, or 70% RH at a temperature of 17 ± 2°C. Either a Rh-coated tip (Rh-tip: SII NanoTechnology Inc., SI-DF3-R, force constant of 1.6 N/m, resonant frequency of 26 kHz, and

tip radius of about 30 nm) or a boron-doped conductive diamond-coated tip (CDT: Nano sensor, boron-doped conductive diamond tip, force constant of 2.2 N/m, resonant frequency of 75 kHz and a tip radius of about 100 nm) was used for the patterning. After patterning, topographic AFM images of the patterned samples were acquired in dynamic mode using a Si probe tip (SII NanoTechnology Inc., SI-DF20-Al, force constant of 12 N/m and resonant frequency of 125 kHz) under a N<sub>2</sub> purged atmosphere.

In order to investigate the relative water meniscus sizes formed at the tip-sample junction under the pattern drawing condition, we performed force curve measurements while applying a tip-sample voltage of 10 V. Force curves, which are acquired by simultaneously measuring the cantilever deflection versus z-piezo elongation, were taken at ten different positions on the ester-SAM sample surface using the Rh-tip or the CDT, in order to avoid effects of any topographical change produced due to the previous force curve measurements. The RH value in the chamber was controlled in the same way during the patterning. The AFM probe was scanned along the z-direction at a rate of 70 nm/s. The pull-off force, that is, the maximum force shown when the AFM tip is separated from the sample surface, was extracted from each of the measured force curves.

### **III. RESULTS AND DISCUSSION**

Figure 2 shows AFM images of fabricated lines on the samples. Protruded



lines are seen in all the images. On scanning probe anodization of a SAM-covered Si sample with a constant bias voltage,<sup>10</sup> organic molecules consisting of the SAM are, first, gradually decomposed, and accordingly, the SAM is degraded. However, in the initial stage the substrate Si does not react at all since the electrochemical species necessary for anodization of Si are almost perfectly blocked by the SAM itself. When the SAM is degraded to some extent due to anodization, the electrochemical species start to reach into the substrate Si, and it begins to be anodized. In the final stage, the decomposition of the SAM is completed if the bias is sufficient. In this stage, only anodization of the substrate Si proceeds until the thickness of the anodic oxide reaches a specific value determined mainly by the bias voltage for anodization. Finally, due to the larger specific volume of Si oxide than Si, a protruded line is fabricated along the tip-scan trace where anodic Si oxide has been formed, as demonstrated in Fig. 2.

Figures 2(a)-(c) show lines fabricated on the methyl-terminated SAM (methyl-SAM) sample using a Rh-tip at RH = 10, 40 and 70%, respectively. The line width increases from 25 nm (10% RH) to 105 nm (70% RH). Figures 2(d)-(f) indicate lines fabricated on the ester-terminated SAM (ester-SAM) sample using the same Rh-tip at RH = 10, 40 and 70%, respectively. The line width increases from 20 nm (10% RH) to 140 nm (70% RH). The results on the carboxyl acid-terminated SAM (carboxyl-SAM) sample are shown in Figs. 2(g)-(i). These lines were fabricated at RH = 10, 40 and 70%, respectively, with the same Rh-tip used for the experiments on the methyl- and ester-SAM

samples. The line width increases from 20 nm (10% RH) to 230 nm (70% RH).

The widths (full width at half maximum) and heights of the lines are summarized in Fig. 3. These values were estimated from ten section profiles of each line using image SXM software (version 1.84). As clearly seen in Fig. 3(a), the degree of the line width increase with RH becomes large depending on the hydrophilicity of the sample surface. Namely, on the hydrophilic sample (carboxyl-SAM: water contact angle of  $53^\circ$ ), the fabricated line becomes wider than that fabricated on the hydrophobic sample (methyl-SAM: water contact angle of  $96^\circ$ ). This tendency is most distinct under the high humidity condition of 70% RH, while the difference is very small under the low humidity condition of 10% RH. The origin of this phenomena is most certainly the size effect of the water meniscus formed at the tip-sample junction. It is known that the tip-anodized Si size is determined by meniscus size.<sup>31</sup> It has also been reported that, on a hydrophobic SAM sample, the anodized line width is almost independent of humidity,<sup>9</sup> while on a hydrophilic oxide surface it shows a strong humidity dependence due to the widely spreading water meniscus under high humidity.<sup>6</sup> It should be noted that, under the low humidity condition of 10% RH, the line width is independent of surface hydrophilicity/hydrophobicity. It is probable that, at this low humidity value, the water meniscus size is primarily governed by the tip size. Consequently, the patterning resolution down to 20 nm was attained regardless of the SAM type. These humidity and surface wettability effects on the water meniscus are schematically illustrated in Figs. 4(a)-(c).

Besides the line width, the line height behavior is summarized in Fig. 3(b) as well. The line height is less dependent on the surface wettability. Under all the humidity conditions, namely, 10, 40 and 70% RH, there are no significant difference in height between the lines fabricated on the methyl-, ester- and carboxyl-SAM samples. Furthermore, line heights fabricated at 40% and 70% RH are almost the same in the range of 2.5 - 3.0 nm, while those at 10% RH are smaller than 1.0 nm. These results can be explained based on the nature of anodization. In anodization at a constant voltage, the oxide thickness grown on a substrate surface first increases with time. However, it reaches a certain limit value determined by the voltage and the substrate material if anodization is prolonged for a sufficient period. Thus, we can conclude as follows. In the center area of each anodized line fabricated at 40% and 70%RH as shown in Figs. 2(b), 2(c), 2(e), 2(f), 2(h) and 2(i), the SAM was completely decomposed and the substrate Si was fully anodized so that the anodic Si oxide thickness in this area reached a limit value at a bias voltage of 10 V. On the other hand, in the case of the anodized lines fabricated at 10% RH as shown in Figs. 2(a), 2(d) and 2(g), anodization was not completed even at the center of each line, probably due to the shortage of adsorbed water which served as the source substance for electrochemical oxidation of SAM and Si.

Figure 5 shows the aspect ratios of the anodized lines as estimated from the results shown in Figs. 4(a) and 4(b). In the case of the Rh-tip patterning, the aspect ratios depend on RH and the surface wettability. The aspect ratios of the

lines fabricated on the methyl-SAM sample, i.e., the most hydrophobic sample, are higher than those of the lines fabricated on the other SAMs which are relatively hydrophilic. In each SAM case, the aspect ratio becomes highest at 40% RH. The combination of proper humidity and hydrophobic surface will provide anodized lines with a higher aspect ratio.

Here we discuss the results obtained using CDT and the ester-SAM sample. As shown Figs. 2(j)-(l), there is no distinct humidity dependence of line width of the anodic patterns fabricated on the ester-SAM sample with a CDT. As plotted in Fig. 3, the width of the anodized lines hardly changes with increasing RH from 10 % to 70 %. Accordingly, their aspect ratios do not change so much. In addition, the widths of the lines anodized by the CDT are comparable or even much smaller than those of the lines anodized by the Rh-tip. At 40% RH, the CDT line width is one fourth of the Rh line width. The difference becomes much greater at 70% RH. The CDT line width is near one tenth of the Rh line width. These results are surprising considering the much larger tip radius of the CDT, i.e., 100 nm compared with that of the Rh-coated tip, i.e., 30 nm. There are two plausible explanations: the CDT surface has a hydrophobic nature<sup>32</sup> and hydrogen evolution ( $2\text{H} + 2\text{e}^- \rightarrow \text{H}_2$ ) as a cathode reaction on the boron-doped diamond surface is slow.<sup>33</sup> It would be considered that the hydrophobic CDT possibly confines the adsorbed water meniscus in a restricted region under the tip as illustrated in Fig. 4(d). The slow hydrogen evolution rate at the cathode electrode, that is, the CDT surface in this case, might result in slow anode

reactions at the sample surface, because the same number of electrons flows through the cathode and anode surfaces according to the basic principle of electrochemistry.

We performed force curve measurements on the ester-SAM sample surface in order to investigate the relative meniscus sizes of adsorbed water under the condition applying a tip-sample voltage of 10 V. A pull-off force was derived from each of the force curves. The pull-off force is considered to contain both the electrostatic force and the meniscus force. We assume that the electrostatic force is constant for the a same AFM probe. Thus, the difference of the pull-off force is considered to indicate a difference of the meniscus force. The results are summarized in Fig. 6. Each value represents an average of ten pull-off forces measured under the same conditions. It should be noted that the absolute pull-off forces are very different between those obtained with the Ph-tip and with the CDT due to the large tip-radius difference, so we cannot compare them directly. We discuss only humidity dependencies of the pull-off forces. As shown in Fig. 6(a), the pull-off force increases with increasing RH, when measured by the Rh-tip. This pull-off force increase, therefore, most likely corresponds to an increase of meniscus size. This result agrees with the result of line widening under higher humidity as shown in Fig. 3(a). Several groups have reported similar force curve experiments with changing bias voltages.<sup>34-36</sup> On the other hand, in the case of the CDT as shown in Fig. 5(b), there is little change in pull-off force versus RH. This can be concluded to indicate no increase in meniscus

size and agrees with the pattern width results.

#### **IV. CONCLUSIONS**

We have studied AFM-based scanning probe anodization of SAM-covered Si samples in terms of the effects of environmental humidity, surface wettability and probe-tip material on widths and heights of drawn lines. The AFM was operated in contact mode during the anodization patterning. We prepared three types of SAMs, that is, methyl-, ester- and carboxyl-terminated SAMs, of which the water contact angles were  $96^\circ$ ,  $73^\circ$  and  $53^\circ$ , respectively, covalently immobilized on Si(111) surface through Si-C bonds. When the Rh-coated AFM tip was used for anodization, the patterned line width was markedly dependent on humidity and surface wettability. Namely, lower RH and/or more hydrophobic surface provided finer patterns. In contrast, when the CDT was used for anodization of the ester-SAM sample, the patterning was less humidity-dependent than with the Rh-coated tip. Furthermore, the CDT was found to enable drawing of lines with a comparable or even thinner width in spite of its tip radius of 100 nm being much larger than that of the Rh-coated tip, i.e., 30 nm. This is primarily ascribable to hydrophobic nature of CDT which might confine the water meniscus in a restricted area. Although, in this study, we were able to draw 20 nm wide lines, the optimization of humidity and surface wettability of both tip and sample will lead to finer patterning.

#### **ACKNOWLEDGMENTS**

The present work was supported by a Grant-in-Aid for the Global COE Program, “International Center for Integrated Research and Advanced Education in Materials Science”, and by KAKENHI (Grant-in-Aid for Scientific Research) No. 19049010 on Priority Area “Strong Photons-Molecules Coupling Fields (470)”, from the Ministry of Education, Culture, Sports, Science and Technology of Japan.

## REFERENCES

- <sup>1</sup>H. Rohrer, Jpn. J. Appl. Phys. **32**, 1335 (1993).
- <sup>2</sup>P. Avoris, Acc. Chem. Res. **28**, 95 (1995).
- <sup>3</sup>R. M. Nyffebegger and R. M. Penner, Chem. Rev. **4**, 1195 (1997).
- <sup>4</sup>C. F. Quate, Surf. Sci. **386**, 259 (1997).
- <sup>5</sup>H. Sugimura, in *Applied Scanning Probe Methods X, Biomimetics and Industrial Applications*, edited by B. Bhushan, H. Fuchs, and M. Tomitori (Springer, 2008), p. 217.
- <sup>6</sup>H. Sugimura, T. Uchida, N. Kitamura, and H. Masuhara, J. Phys. Chem. **98**, 4352 (1994).
- <sup>7</sup>S. Krämer, R. R. Fuierer, and C. B. Gorma, Chem. Rev. **103**, 4367 (2003).
- <sup>8</sup>H. Sugimura, Int. J. Nanotechnology **2**, 314 (2005).
- <sup>9</sup>H. Sugimura, K. Okiguchi, and N. Nakagiri, Jpn. J. Appl. Phys. **35**, 3749 (1996).
- <sup>10</sup>H. Sugimura, T. Hanji, K. Hayashi, and O. Takai, Ultramicroscopy **91**, 221 (2002).
- <sup>11</sup>C. R. K. Marrian, F. K. Perkins, S. L. Brandow, T. S. Koloski, E. A. Dobisz, and J. M. Calvert, Appl. Phys. Lett. **64**, 390 (1994).
- <sup>12</sup>S. L. Brandow, J. M. Calvert, E. S. Snow, and P. M. Campbell, J. Vac. Sci. Technol. A **15**, 1455 (1997).
- <sup>13</sup>H. Sugimura, O. Takai, and N. Nakagiri, J. Electroanal. Chem. **473**, 230 (1999).



- <sup>14</sup>Q. Li, J. Zheng, and Z. Liu, *Langmuir* **19**, 166 (2003).
- <sup>15</sup>H. Sugimura and N. Nakagiri, *J. Am. Chem. Soc.* **119**, 9226 (1997).
- <sup>16</sup>H. Sugimura, T. Hanji, K. Hayashi, and O. Takai, *Adv. Mater.* **14**, 524 (2002).
- <sup>17</sup>R. Maoz, S. R. Cohen, and J. Sagiv, *Adv. Mater.* **11**, 55 (1999).
- <sup>18</sup>S. Hoepfner, R. Maoz, S. R. Cohen, L. Chi, H. Fuchs, and J. Sagiv, *Adv. Mater.* **14**, 1036 (2002).
- <sup>19</sup>M. R. Linford, P. Fenter, P. M. Eisenberger, and C. E. D. Chidsey, *J. Am. Chem. Soc.* **117**, 3145 (1995).
- <sup>20</sup>P. Wagner, S. Nock, J. A. Spudich, W. D. Volkmuth, S. Chu, R. L. Cicero, C. P. Wade, M. R. Linford, and C. E. D. Chidsey, *J. Struct. Biol.* **119**, 189 (1997).
- <sup>21</sup>M. M. Sung, G. J. Kluth, O. W. Yauw, and R. Maboudian, *Langmuir* **13**, 6164 (1997).
- <sup>22</sup>N. Saito, S. Youda, K. Hayashi, H. Sugimura, and O. Takai, *Surf. Sci.* **532**, 970 (2003).
- <sup>23</sup>M. Ara, H. Graaf, and H. Tada, *Appl. Phys. Lett.* **80**, 2565 (2002).
- <sup>24</sup>B. Pignataro, A. Licciardello, S. Cataldo, G. Marletta, *Mater. Sci. Eng. C* **23**, 7 (2003).
- <sup>25</sup>Y. Menglong, Z. Zhikun, L. Yaqing, and Z. Bailin, *Nanotechnology* **17**, 330 (2006).
- <sup>26</sup>J. Han, H. Sano, Y. J. Kim, T. Ichill, K. Murase, and H. Sugimura (to be published).
- <sup>27</sup>H. Sugimura, A. Hozumi, T. Kameyama, and Osamu Takai, *Surf. Interf. Anal.*

- 34**, 550 (2002).
- <sup>28</sup>H. Sugimura, H. Sano, K. -H. Lee, and K. Murase, *Jpn. J. Appl. Phys.* **45**, 5456 (2006).
- <sup>29</sup>T. Strother, W. Cai, X. Zhao, R. J. Hamers, and L. M. Smith, *J. Am. Chem. Soc.* **122**, 1205 (2000).
- <sup>30</sup>B. Fabre and F. Hauquier, *J. Phys. Chem. B* **110**, 6848 (2006).
- <sup>31</sup>R. Garcia, M. Calleja, and H. Rohrer, *J. Appl. Phys.* **86**, 1898 (1999).
- <sup>32</sup>M. J. Schmitz, C. R. Kinser, N. E. Cortes, and M. C. Hersam, *Small* **3**, 2053 (2007).
- <sup>33</sup>H. B. Martin, A. Argoitia, U. Landau, A. B. Anderson, and J. C. Angus, *J. Electrochem. Soc.* **143**, L133 (1996).
- <sup>34</sup>S. F. Lyuksyutov, P. B. Paramonov, I. Dolog, and R. M. Ralich, *Nanotechnology* **14**, 716 (2003).
- <sup>35</sup>C. Martin, F. P. Murano, and J. A. Dagata, *IEEE* 781 (2003).
- <sup>36</sup>S. Hoepfener, J. H. K. van Schaik, and U. S. Schubert, *Adv. Funct. Mater.* **16**, 76 (2006).

Fig. 1. Schematic illustration of the sample preparation procedures. (a) Oxide-covered Si substrate, (b) hydrogen-terminated Si(111) substrate, (c) methyl-terminated SAM, (d) ester-terminated SAM and (e) carboxyl-terminated SAM.

Fig. 2. Topographic images acquired by dynamic-mode AFM for the patterned regions. Fabricated lines on the methyl-SAM sample at RH = (a) 10%, (b) 40% and (c) 70% using the Rh-tip. Fabricated lines on the ester-SAM sample at RH = (d) 10%, (e) 40% and (f) 70% using the Rh-tip. Fabricated lines on the carboxyl-SAM sample at RH = (g) 10%, (h) 40% and (i) 70% using the Rh-tip. Fabricated lines on the ester-SAM sample at RH = (a) 10%, (b) 40% and (c) 70% using the CDT.

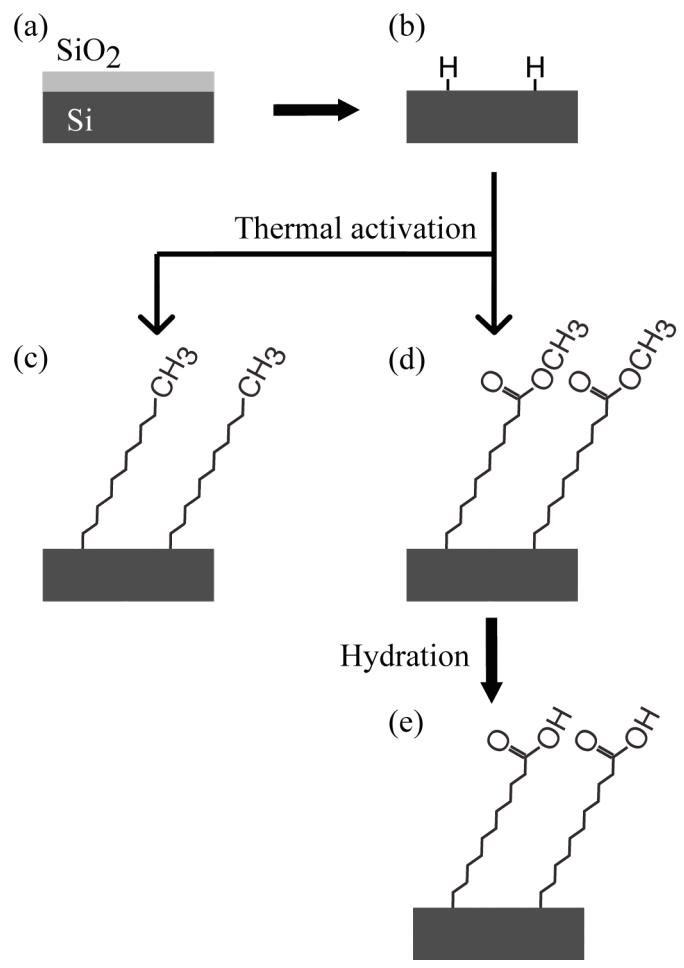
Fig. 3. Humidity and wettability effects on anodization patterning of the SAM samples. (a) Width and (b) height vs. RH. Solid and dotted lines correspond to the results patterned by the Rh-tip and CDT, respectively.

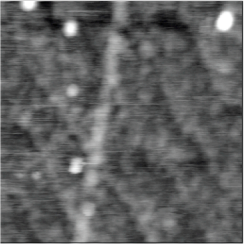
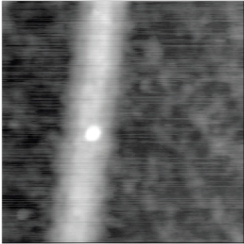
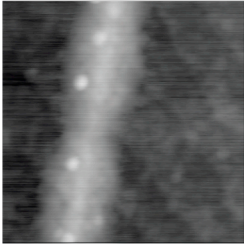
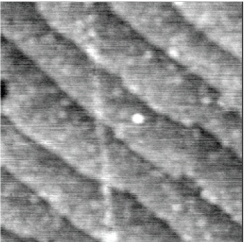
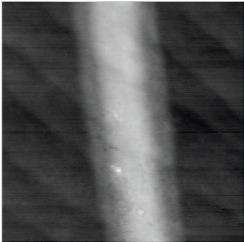
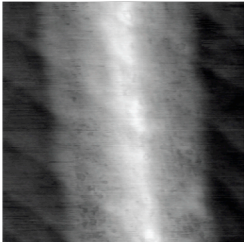
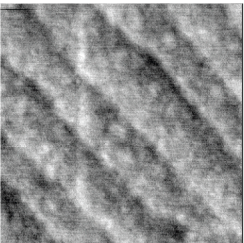
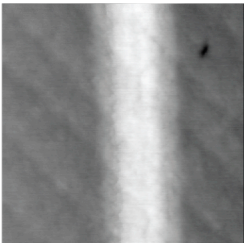
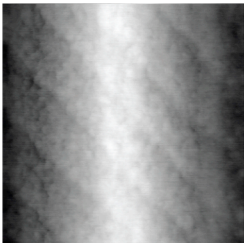
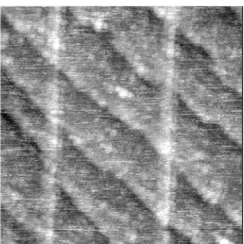
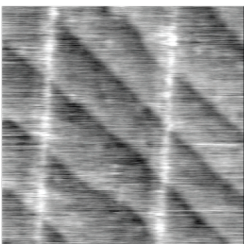
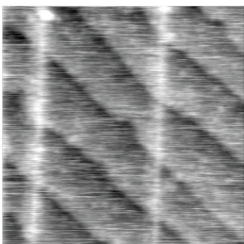
Fig. 4. Schematic illustration of the behavior of water meniscus dependent on humidity and wettability of sample and tip surfaces. Outermost lines drawn at the tip-sample junctions indicate water menisci under a high humidity condition, while innermost lines demonstrate water menisci under a low humidity condition. The junctions between a Rh-tip and (a) methyl-, (b) ester- or (c) carboxyl-SAM samples. (d) The junction between a CDT and an ester-

SAM sample.

Fig. 5. Aspect ratios of the fabricated lines shown in Fig. 2 as functions of humidity. Solid and dotted lines correspond to the results patterned by the Rh-tip and CDT, respectively.

Fig. 6. Humidity dependence of pull-off force on the ester-SAM sample acquired by (a) the Rh-tip and (b) the CDT with a sample bias voltage of 10 V.



		10% RH	40% RH	70% RH
Rh-tip	CH <sub>3</sub>	(a) 	(b) 	(c) 
	COOCH <sub>3</sub>	(d) 	(e) 	(f) 
	COOH	(g) 	(h) 	(i) 
CDT	COOCH <sub>3</sub>	(j) 	(k) 	(l) 

100 nm

